DESDE 2013
https://repository.uaeh.edu.mx/revistas/index.php/icbi/issue/archive
Pädi Boletín Científico de Ciencias Básicas e Ingenierías del ICBI
ISSN: 2007-6363

Publicación Semestral Pädi Vol. 14 No. Especial (2026) 142-148

Metal phthalocyanines as organic semiconductor layer in optoelectronic devices
Ftalocianinas metálicas como capa orgánica semiconductora en dispositivos optoelectrónicos

I.S. Rincón-Von Pastor[a,*], L.A. Cantera-Cantera[a,b], M.E. Sánchez-Vergara[a]

[a] *Faculty of Engineering, Universidad Anáhuac México, Av. Universidad Anáhuac 46, Col. Lomas Anáhuac, Huixquilucan C.P. 52786, México.*
[b] *Instituto Politécnico Nacional, Departamento de Ingeniería en Control y Automatización, ESIME-Z, Av. Luis Enrique Erro S/N, Gustavo A. Madero, Zacatenco, Ciudad de México 07738, México.*

Resumen

Se fabricaron dispositivos con ftalocianinas metálicas donantes (MFt; M=Co, Cu) y el aceptor electrónico tetraciano-π-quinodimetano (TCNQ), como componentes de la capa activa con arquitectura de heterounión en masa (HM). Inicialmente, estas capas MFt+TCNQ se estudiaron en su comportamiento óptico y posteriormente, se fabricaron los dispositivos utilizando óxido de indio y estaño (ITO: $In_2O_3(SnO_2)_x$) como ánodo, y Ag como cátodo. Para optimizar los dispositivos, se adicionaron con arquitectura de heterojunción plana (HP), capas transportadoras de huecos y electrones de pentaceno y batocuproína respectivamente. El estudio del comportamiento eléctrico mostró que tanto la irradiación con diferentes longitudes de onda, como el cambio en la polaridad de los electrodos, modifica el transporte de cargas, lo anterior está relacionado con el tipo de ftalocianina del dispositivo. En el caso del dispositivo con CoFt el comportamiento es óhmico, y en el dispositivo con CuFt este comportamiento se da a bajos voltajes, y a mayores, el comportamiento cambia a corriente limitada por carga espacial (SCLC).

Palabras Clave: Ftalocianina Metálica, Película Semiconductora, Dispositivo Orgánico, Comportamiento Eléctrico.

Abstract

Devices were fabricated using donor metal phthalocyanines (MPc; M = Co, Cu) and the electron acceptor tetracyano-π-quinodimethane (TCNQ) as components of the active layer in a bulk heterojunction (BHJ) architecture. Initially, the optical behaviour of the MPc+TCNQ layers was studied, followed by the fabrication of the devices employing indium tin oxide (ITO: $In_2O_3(SnO_2)_x$) as the anode and silver (Ag) as the cathode. To optimize device performance, additional layers were introduced in a planar heterojunction (PHJ) configuration, using pentacene and bathocuproine as the hole and electron transport layers, respectively. The study of the electrical behaviour revealed that both light irradiation at different wavelengths and variations in electrode polarity affect charge transport, which is correlated with the type of phthalocyanine employed. In the case of the device containing CoPc, ohmic behaviour was observed, whereas the device with CuPc exhibited ohmic behaviour at low voltages, transitioning to space-charge-limited current (SCLC) conduction at higher voltages.

Keywords: Metal Phthalocyanine, Semiconductor Film, Organic Device, Electrical Behaviour.

1. Introduction

Metal-free phthalocyanine (H_2Pc) can be used as a semiconducting material in organic electronic devices (Saady et al., 2023) and because of its sensitivity and selectivity towards certain gases, H_2Pc is a good candidate for gas sensing applications (Yabaş et al., 2021). However, H_2Pc is a divalent acid; upon dissociating, it becomes the ligand $[HPc]^-$ or $[Pc]^{2-}$ which are strong binders for metal ions (Limin & Xian-Fu, 2022) and form the metal phthalocyanines (MPcs). MPcs belong to the class of 18π-electron aromatic systems with two covalent bonds and two coordination bonds chelating a metal centre (Cranston & Lessard, 2021; Muranaka & Uchiyama, 2021). An MPc consists of four isoindole units connected through nitrogen atoms of the tetrabenzoporphyrazine macrocycle. Modification of the π-framework is a way of

*Autor para la correspondencia: ingrid.rincon@anahuac.mx,
Correo electrónico: ingrid.rincon@anahuac.mx (Ingrid Sofía Rincón-von Pastor), calberto@anahuac.mx (Luis Alberto Cantera-Cantera), maria.elena@anahuac.mx (María Elena Sánchez-Vergara).

Historial del manuscrito: recibido el 19/06/2025, última versión-revisada recibida el 12/12/2025, aceptado el 08/02/2026, publicado el 25/03/2026. **DOI:** https://doi.org/10.29057/icbi.v14iEspecial.15346

altering the electronic structure of molecules, and many types of modified phthalocyanines have been developed. For example, expansion or contraction of π-conjugation, symmetry lowering, and heteroatom replacement are used to alter their electronic and optical properties (Kudrevich & Van Lier., 1996; Claessens et al., 2002; Kobayashi, 2002). Due to the above, MPcs are utilised in various types of organic sensing devices, including resistive and capacitive sensors, solid-state ionic sensors, devices based on field-effect organic transistors, and light emitting organic diodes (Basova, 2024). Furthermore, thanks to the fine-tuning of their energy levels, simple synthesis, good thermal stability, excellent reproducibility, and relatively easy film-forming process, one of the specific uses of MPc films is as active layers in the manufacture of organic devices (Yu, Liu, et al., 2015). More than 70 metal ions have been introduced into the phthalocyanine cavity; hence, the role of MPcs as active layers of organic devices is important and different types of phthalocyanine-based organic devices have been studied (Basova, 2024; Kumar, 2020; Gounden, 2020).

Among the most common MPcs, copper phthalocyanine (CuPc) is an organic semiconductor notable for its properties and characteristics, such as its high thermal and chemical stabilities, which allow it to be processed as a thin film. Its controllable photophysical, photochemical, redox, and coordination properties, in addition to the possibility of modifying its semiconductor behaviour, are due to the presence of radicals and functional groups in its molecular structure (Hains, Liang. 2010; Christie, & Abel, 2021; Demir et al. 2024). Moreover, CuPc offers a wide absorption spectrum in the ultraviolet–visible spectrum (Ali et al., 2020; Caplins, Mullenbach, Holmes, 2016), and long exciton diffusion length (8 nm–68 nm) (Hains, Liang. 2010; Stübinger & Brütting, 2001). Additionally, CuPc, known for its high electrical conductivity, is chosen for the construction of organic devices as a p-type active layer (Demir et al. 2024). However, improvements in turn-on voltage and luminance have been observed in organic light-emitting diodes (OLEDs) when using a cobalt phthalocynine (CoPc) layer (Zhu et al., 2001; Kao et al., 2005; Ma et al., 2015; Lee et al., 2012). The driving voltages of the MPc electroluminescence devices are found to decrease in the order of CuPc < CoPc < H_2Pc, this is in line with the order of Highest Occupied Molecular Orbital (HOMO) levels of MPcs (Zhu et al, 2001). CoPc is stable in water and air, as well as thermally stable, hence it can be sublimed and form thin films on a variety of substrates (Gravano, et al., 1991). Like CuPc, CoPc is used in many organic electronic devices as a p-type semiconducting film. Charge transport in films is generated due to the alignment of MPcs molecules, which is achieved by the overlap between π-orbitals of adjacent molecules. As a result of this alignment, one-dimensional wires are formed, meaning that films with a columnar structure feature anisotropic charge mobility (Özdemir et al., 2022; Zhang et al., 2020). Thus, the importance of the study of CuPc and CoPc as active layers in organic optoelectronic devices is highlighted.

In the present work, simple devices based on donor MPc (M = Co, Cu) and the electron acceptor tetracyano-p-quinodimethane (TCNQ) as components of the active layer were deposited. Subsequently, to determine the active layer conditions that generate the highest operating efficiency, devices were fabricated with both bulk heterojunction (BHJ) and planar heterojunction (PHJ) architectures. The MPc+TCNQ active layer was prepared with BHJ and its integration into the device with the hole and electron transport layers (pentacene and bathocuproine respectively) was deposited by PHJ. Due to its optical and electrical properties, indium tin oxide coated PET and glass slides (ITO: $In_2O_3{\cdot}(SnO_2)_x$) were used as a transparent anode. The transparency of ITO is >85% through the visible region of the spectrum, which allows efficient light-harvesting by the active layer of the device. Silver electrodes (Ag) were deposited on the devices to function as cathodes. The work function (φf) of Ag is closer to that of ITO and would provide a field that promotes hole collection at the ITO anode and electron collection at the Ag cathodes.

2. Experimental Method

The cobalt (II) phthalocyanine (CoPc: $C_{32}H_{16}CoN_8$), copper (II) phthalocyanine (CuPc: $C_{32}H_{16}CuN_8$), 7,7,8,8-tetracyanoquinodimethane (TCNQ: $C_{12}H_4N_4$), pentacene ($C_{22}H_{14}$) and bathocuproine (BCP: $C_{26}H_{20}N_2$) used in this study (see Figure 1), were acquired from the commercial supplier Sigma-Aldrich and used without additional purification. To verify the main functional groups of the organic compounds used, Infrared (IR) spectroscopy analysis was performed on a Nicolet iS5-FT spectrometer.

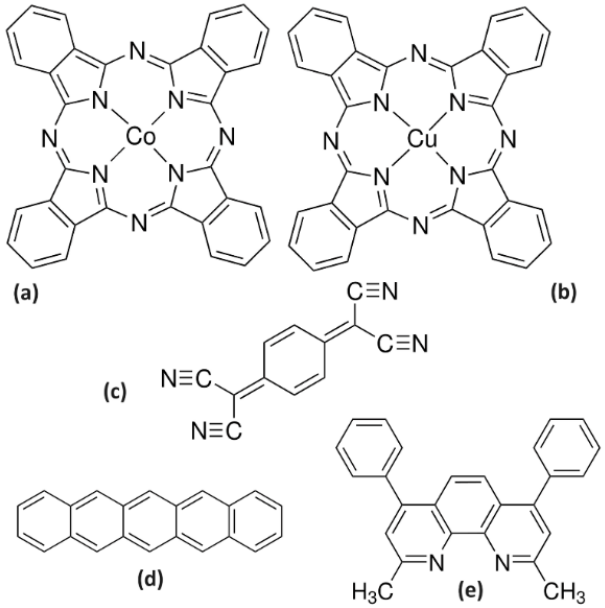

Figure 1: Structure of (a) CoPc, (b) CuPc, (c) TCNQ, (d) pentacene and (e) BCP.

The active layer was prepared in two steps: the formation of the bulk heterojunction (BHJ) n-p and the deposition of the film. The BHJ n-p was obtained by a simple reaction under the mass ratio of 1:2 of TCNQ and MPc (M=Co, Cu) respectively in absolute MeOH in a heated Monowave 50 reactor. The reactor system employed a borosilicate glass vial with integrated temperature monitoring and was operated at a constant pressure of 20 bar. Each reaction was maintained for 30 minutes, after which the resulting compounds were purified by washing with methanol (MeOH) and dried under vacuum to isolate the BHJ as solid powders. The deposition of the BHJ films took place using a high-vacuum sublimation technique

onto different substrates: Corning glass, indium tin oxide ($In_2O_3 \cdot (SnO_2)_x$) coated glass slide (glass-ITO), and indium tin oxide coated polyethylene terephthalate film (PET-ITO). Sublimation and deposition of the films was conducted inside a high vacuum chamber with a molybdenum boat. The evaporation rate (5 Å/s), temperature (280°C) and pressure (1×10^{-5} torr) in the vacuum chamber were the same for all the deposition processes. Each layer thickness was monitored by a quartz crystal microbalance connected to a thickness sensor. The absorbance and transmittance in the range between 200 and 800 nm of the films deposited on Corning glass were obtained with a UV-vis spectrophotometer, model Evolution 220 from Thermo Scientific.

For electrical characterization, BHJ films were prepared according to the scheme in Figure 2a, with ITO used as the anode and Ag acting as the cathode. The optimized device with the pentacene and BCP layers is presented in the schematic in Figure 2b. It is important to mention that the devices were manufactured on two types of substrates: rigid, on glass; and flexible, on PET. The current-voltage (I-V) measurements were performed employing a programmable voltage source, a Keithley 4200-SCS-PK1 auto-ranging pico-ammeter. A Next Robotix sensing station with lighting and temperature controller circuits that emit electromagnetic radiation between the UV an IR wavelength interval was also used. The I-V measurements were made in a range between -1.1 V and 1.1 V with a step of 0.05 V, drawing a total of 45 points. Delay and hold times were 0 s. To evaluate the device's ambipolarity, the roles of the electrodes were interchanged. Initially the ITO acted as an anode while Ag acted as the cathode. Subsequently, the polarity of the electrodes was reversed.

The reflectance R in the range between 200 and 800 nm was detected utilizing a Unicam 300 double-beam spectrophotometer equipped with an integrating sphere and an 8° near-normal reflectometer.

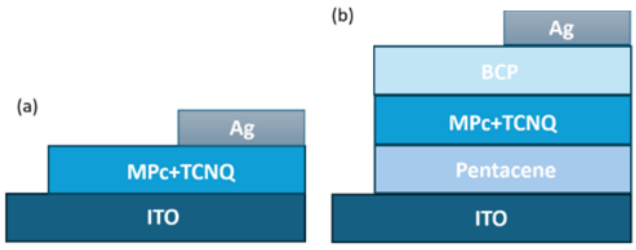

Figure 2: Schematics of the (a) ITO/MPc+TCNQ/Ag, and (b) ITO/Pentacene/MPc+TCNQ/BCP/Ag devices.

3. Results and Discussion

In the context of incorporating a BHJ film into optoelectronic devices whose operation relies on radiation absorption or emission, transmittance and absorbance emerge as critical properties. These characteristics play a fundamental role in determining the optimal compatibility and performance of the film within a given device configuration. Regarding this, in Figure 3, both the transmittance and absorbance of the BHJ films are observed, where a similar behaviour is evident in the two MPc+TCNQ films. The maximum transmittance for CuPc+TCNQ of 78% at 800 nm and 68% for CoPc+TCNQ at 800 nm makes these films promising candidates to be incorporated as components of optoelectronic devices that require transparent circuits at long wavelengths (Thomas, 1997). On the other hand, the absorbance records the different electronic transitions that take place in the BHJ films due to the absorption of radiation of different wavelengths. In the absorbance curves, both films present small transitions between 300 and 400 nm, with a slight red shift by the CoPc+TCNQ film. This shift is usually attributed to the intermolecular interactions of the BHJ film (Miao et al., 2006; Braitbart et al., 1988). From the absorbance, the value of the optical bandgap, E_{opt}, is estimated, which is attributed to the lower energy transition that takes place by absorption of a photon. There are several methods to calculate E_{opt}, the most used is the extrapolation of the linear section of the skirt of the lower energy band, up to the point of intersection with the abscissa axis. With this wavelength value, the optical bandgap, E_{opt}, is obtained from:

$$E_{opt} = \frac{hc}{\lambda} \quad (1).$$

Where h is Planck's constant, c the speed of light in vacuum and λ the wavelength. The estimated values for each film are presented in Table 1.

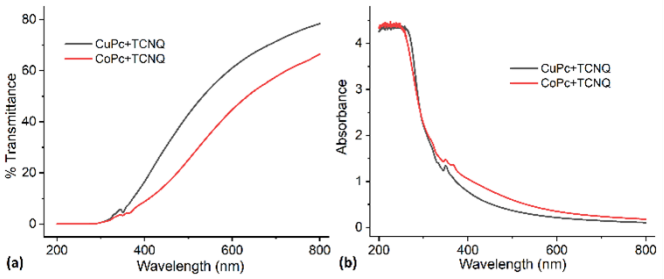

Figure 3: (a) Transmittance and (b) Absorbance for CoPc+TCNQ and CuPc+TCNQ films.

Table 1: Optical bandgap E_{opt} for BHJ films

Film	E_{opt} (eV)
CoPc+TCNQ	3.70
CuPc+TCNQ	3.86

PET/ITO/MPc (M=Co, Cu) + TCNQ/Ag devices were manufactured, with the purpose of analysing their electrical behaviour under different lighting conditions, including infrared and ultraviolet of the electromagnetic spectrum. Figure 4 shows the current-voltage (I-V) graphs for the device with the CoPc+TCNQ film (Figure 4a) and for the device with the CuPc+TCNQ film (Figure 4b). Although both devices exhibit changes in charge transport under different lighting conditions, and the reversal of electrode polarity also affects charge movement, their electrical behaviours differ significantly. Such disparity is closely linked to the specific MPc compound employed in the active layer of each device. In the device with the CoPc film, the electric current is significantly affected by the direction of charge flow, whether from ITO to Ag or vice versa. In the first instance, the behaviour of the current is ohmic; in the latter, and especially for normal or natural lighting conditions of the device, at voltages less than 0.75V, the behaviour is ohmic, while at voltages greater than 0.75 V its behaviour changes to space-charge-limited current (SCLC). This change may be due to the fact that at low voltages, a saturation of charges is generated in certain areas of the CoPc+TCNQ film, which prevents the continuous flow of charges until, with the increase in voltage,

they continue to flow, although not with the same slope or I-V relationship, but a slowdown occurs in the electrical transport and from 1.7x10^{-3}V it drops slightly to 1.6x10^{-3}V. This device can be found within the so-called electron- or hole-only devices, in which, by choice of the anode and cathode, either only electrons or holes are injected into the semiconductor. The maximum electrostatically allowed current in such a device is limited by the build-up of space charge (Alvar et al., 2020). In the case of the device manufactured with the CuPc+TCNQ film, ohmic behaviour is observed for white, yellow, orange, red, blue and UV illumination. However, in natural and green lighting conditions, for voltages higher than 0.5V, the current flow becomes irregular and when the device is subjected to dark conditions, the behaviour changes significantly. As the voltage increases up to 0.55V, its behaviour is ohmic, subsequently a drop is generated in the transported current up to 0.7 V, and at higher voltages the current increases again and in fact reaches the highest value of 1.2x10^{-3}A.

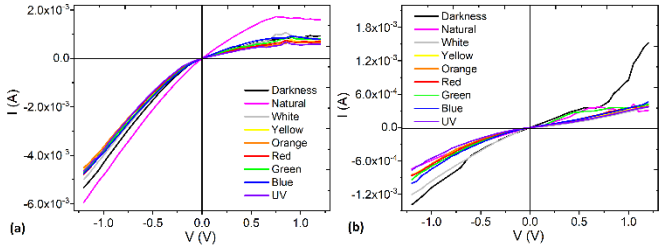

Figure 4: I-V behaviour for ITO/MPc + TCNQ/Ag (a) M = Co and (b) M = Cu devices.

Reflectance (R) is a key optical parameter in optoelectronic devices. High R values can lead to reduced light absorption, ultimately lowering the conversion efficiency of solar energy into electricity and, consequently, the overall device performance. In organic solar cells, for instance, the surface reflectance directly influences the amount of light entering the device; with sensors, the *R* of the surface can affect the amount of light detected. Meanwhile, in OLEDs, a high *R* inside the device can cause unwanted reflections and reduce image contrast. For this reason, the *R* was evaluated in the complete systems: pentacene/MPc (M=Co, Cu) + TCNQ/BCP. The spectral distribution of *R* as a function of wavelength λ, for the deposited systems are shown in Figure 5a. The diffuse reflectance occurs in the range of 200 to 800 nm, where an interaction between electromagnetic radiation and the deposited systems is observed.

The R spectra presented in Figure 5a illustrate the proportion of incident radiation reflected by each system. Notably, the CuPc-based film demonstrates higher reflectance than the CoPc-based film, with both exhibiting a maximum at 400 nm (35% for CuPc and 20% for CoPc). This elevated reflectance at 400 nm in the CuPc system may contribute to lower photon absorption, potentially decreasing the device's photovoltaic performance relative to its CoPc counterpart. At wavelengths below 350 nm, both systems exhibit comparable behaviour, with reflectance near 5%, indicating efficient absorption of high-energy photons capable of promoting electron–hole pair generation. Furthermore, it is possible to conclude that the wavelength corresponding to the band gap energy, is most likely located between ~380 nm (yhe beginning of absorption of radiation by sample) and ~350 nm (the value from which almost all radiation is absorbed). However, in the vicinity of the absorption edges (350 and 380 nm), there is an influence of the band tails, which cannot be assessed by diffuse reflectance measurements (Landi et al., 2021).

To get the band gap energy in the two systems, the Kubelka-Munk function F(KM) was used (Landi et al., 2021). This function was obtained from the data of the diffuse reflectance spectrum, and the value of the band gap can be estimated from the same spectrum using the Tauc equation (Landi et al., 2021; Tauc, 1968; Tauc & Menth, 1972):

$$hva = A\left(hv - E_g\right)^p \quad (2).$$

Where *hv* is the photon energy, α is the absorption coefficient, *A* is a proportionality constant, E_g is the forbidden energy band, and the exponent p depends on the band structure of the semiconductor. $P = 1/2$ for allowed transitions occurring at a direct band gap, while $p = 2$ for allowed transitions near an indirect gap where the participation of phonons is required (Landi et al., 2021). In this case, due to the BHJ and PHJ architectures and the different composition of each layer in the pentacene/MPc (M=Co, Cu) + TCNQ/BCP systems, they are considered *allowed transitions* for an indirect gap, referring to amorphous systems. For amorphous systems, the density of states is non-zero inside the band gap, with disorder-induced band tails, so the band bandgap width is not well defined. Band tail states are electronic states located just above the valence band or just below the conduction band. These states typically arise from a structural, impurity, and/or compositional disorder (Wager, 2017). Based on the above, the coefficient α is directly proportional to F(KM), and in the Tauc equation (2), α can be replaced by this function as follows:

$$(hv \times F(KM)) = A\left(hv - E_g\right)^p \quad (3).$$

As discussed previously, in the vicinity of the absorption edges (350 and 380 nm), there is an influence of the band tails, which cannot be assessed by diffuse reflectance measurements. Therefore, the procedure consists in plotting $(hv \times \mathrm{F(KM)})^{1/2}$ versus *hv* fitting the linear portion of this curve with a straight line, where the interception provides the numerical value for *Eg* (Landi et al., 2021). Based on the F(KM) data, Figure 5b shows a plot of $(hv \times \mathrm{F(KM)})^{1/2}$ as a function of the incident photon energy. The band gap values for both pentacene/MPc (M = Co, Cu) + TCNQ/BCP systems were determined within the wavelength range of ~350 nm (3.54 eV) to ~380 nm (3.26 eV), yielding an average band gap of approximately 3.3 eV with a negligible difference (~0.02 eV). Based on these band gap and reflectance (R) results, it is inferred that these systems are viable for integration into optoelectronic devices such as organic solar cells and OLEDs. Although the maximum reflectance ranges from 20% to 35%, practical deployment could benefit from anti-reflective coatings (e.g., silicon oxide or silicon nitride), which reduce reflectance and enhance photon absorption. The uniformity of band gap values further supports effective charge transport across the bulk and planar heterojunction layers.

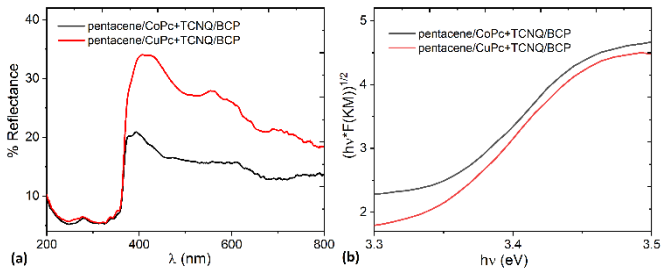

Figure 5: (a) Reflectance spectra and (b) (hν x F(KM))$^{1/2}$ vs hν of pentacene/MPc + TCNQ/BCP systems.

The electrical behaviour of pentacene/MPc (M = Co, Cu) + TCNQ/BCP on both rigid (glass) and flexible (PET) substrates was evaluated, utilising the ITO and Ag electrodes. Figure 6 shows the device structure as an energy-level diagram. It is proposed that ITO acts as an anode or hole injector, with work function, Φf = 4.8 eV, whereas the Ag electrode acts as cathode or electron injector, with a work function of Φf = 4.2 eV. The cathode extracts the electrons from the BCP, which is the electron-carrier layer. This molecule, with its LUMO (3 eV) aligned to the LUMO of the TCNQ (4.2 eV), facilitates the transport of electrons that the TCNQ attracts from the MPc donor. The HOMO of MPc (5.2/5 eV) and the HOMO of pentacene (4.9 eV) present a suitable energy correspondence, which allows the pentacene to facilitate the transport of the holes injected by the anode.

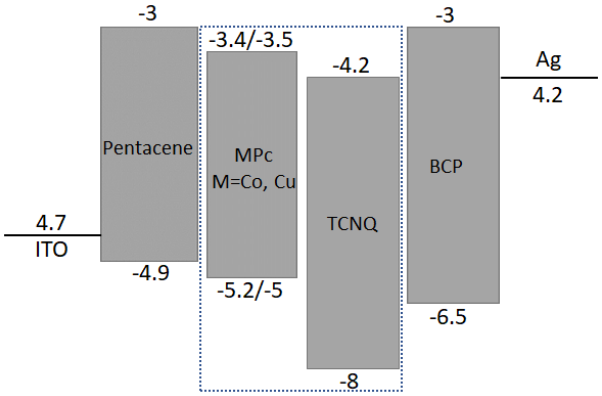

Figure 6: Structure of device, the active layer of which was composed of MPc film doped with TCNQ with HOMO and LUMO levels shown in eV.

The electrical characterization of the fabricated devices was performed by applying a voltage range of -1 V to 1 V, while measuring the current density under various lighting and temperature conditions. Figure 7 shows the current density–voltage (J-V) curves of the devices under different light sources, with the ambient temperature controlled. It is important to mention that, in total, four different devices were evaluated, pentacene/MPc (M = Co, Cu) + TCNQ/BCP (7a) M=Cu on glass, (7b) M = Co on glass, (7c) M = Cu on PET, (7d) M = Co on PET. This evaluation was conducted with the purpose of studying the effect that the type of substrate (rigid or flexible) has on the performance of the devices.

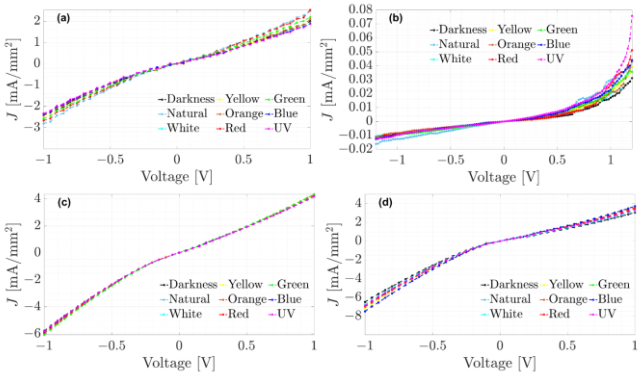

Figure 7: J-V curves at room temperature of pentacene/MPc (M = Co, Cu) + TCNQ/BCP (a) M=Cu on glass, (b) M = Co on glass, (c) M = Cu on PET, (d) M = Co on PET

The electrical conduction results shown in Figure 7, indicate that the device PET/pentacene/CuPc+TCNQ/BCP/Ag (Figure 7c) exhibits a linear or ohmic behaviour, where the average slope in the ohmic region of the positive quadrant is 4.2×10^{-6}. Furthermore, its electrical response remains unaffected by the different lighting conditions. On the other hand, the PET/pentacene/CoPc+TCNQ/BCP/Ag device (Figure 7d) also displays ohmic behaviour with an average slope of 3.39×10^{-6}. However, its electrical conduction shows a slight variation under different lighting conditions, compared with the behaviour observed in the CuPc-based device. The devices fabricated on glass exhibited different behaviors. Notice that the J-V curves of the glass/pentacene/CuPc+TCNQ/BCP/Ag device (Figure 7a) exhibit an ohmic behaviour, whereas the glass/pentacene/CoPc+TCNQ/BCP/Ag device displays a quadratic behaviour or space-charge-limited current (SCLC) regime (Figure 7b) in the positive quadrant. Nevertheless, both devices present conduction variations under different lighting conditions.

To analyse the conduction behaviour of the devices under different temperatures, the electrical characterization was performed under ambient light, applying a voltage from -1 V to 1 V while varying the ambient temperature. Figure 8 shows the J-V curves under different temperature conditions.

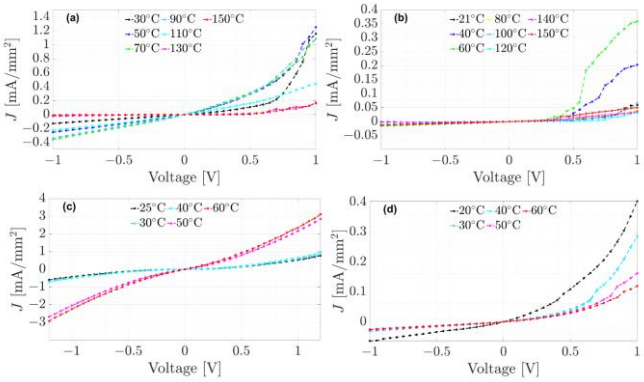

Figure 8: J-V curves for different temperatures of pentacene/MPc (M = Co, Cu) + TCNQ/BCP (a) M=Cu on glass, (b) M = Co on glass, (c) M = Cu on PET, (d) M = Co on PET

As shown in Figure 8, the temperature range used during the tests was from 20 °C to 150 °C. Compared to the results in Figure 7, it is evident that electrical conduction was

significantly affected by temperature, as the behaviour in the positive quadrant is no longer ohmic for all the evaluated devices. Conversely, a decrease in current density was observed for the glass/pentacene/CuPc+TCNQ/BCP/Ag (Figure 8a), PET/pentacene/CuPc+TCNQ/BCP/Ag (Figure 8c), and PET/pentacene/CoPc+TCNQ/BCP/Ag (Figure 8d) devices compared to the results in Figures 7a, 7c, and 7d, respectively.

In contrast, the glass/pentacene/CoPc+TCNQ/BCP/Ag device (Figure 8b) exhibited an increase in current density at temperatures of 40 °C and 60 °C. It is worth noting that the devices fabricated on glass demonstrated a better performance at elevated temperatures than those on PET. For this reason, in Figures 8c and 8d (PET-based devices), the highest temperature reported is 60 °C, whereas for the glass-based devices (Figures 8a and 8b), testing extended up to 150 °C. However, within the tested temperature range, the PET-based devices (Figures 7c and 7d) exhibited higher current density than the glass-based devices (Figures 7a and 7b).

4. Conclusions

In the present work, devices based on MPc (M = Co, Cu) and TCNQ as components of the active layer were fabricated. The devices optical and electrical properties, alongside their observed thermal response, position them as a promising candidate in various areas. Their high transmittance in long-wavelength regions, makes them ideal for applications where transparency in the red and near-infrared is important. The consistent bandgap value of approximately 3.3 eV is a key parameter that allows them to facilitate efficient charge transport in heterojunction architectures, such as solar cells, light sensors and photoreceptors.

Regarding the electrical characterization, the following key points can be highlighted about the performance of the devices: 1) All devices exhibited minimal variations in electrical conduction when exposed to different lighting conditions. In particular, the PET/pentacene/CuPc+TCNQ/BCP/Ag device demonstrated the most stable response. 2) Exposure to varying temperatures generally led to a decrease in current conduction. However, the PET/pentacene/CuPc+TCNQ/BCP/Ag and PET/pentacene/CoPc+TCNQ/BCP/Ag devices demonstrated high current density within the tested temperature ranges, when compared to the devices on glass.

Acknowledgments

I.S.R.v.P. and M.E.S.V. acknowledge financial support from Anahuac Mexico University, Project number PI0000331.

References

Ali, A., Said, A. D., Khayyat, M., Boustimi, M., Seoudi, R., Improving the efficiency of the organic solar cell (CuPc/C60) via PEDOT: PSS as a photoconductor layer doped by silver nanoparticles, Results in Physics 16 (2020) 102819.

Alvar, M. S., Blom, P. W. M., & Wetzelaer, G. A. H. (2020). Space-charge-limited electron and hole currents in hybrid organic-inorganic perovskites. Nature Communications, 11(1). https://doi.org/10.1038/s41467-020-17868-0

Basova, T. (2024). Phthalocyanine and Porphyrin Derivatives and Their Hybrid Materials in Optical Sensors Based on the Phenomenon of Surface Plasmon Resonance. Chemosensors, 12(4), 56. https://doi.org/10.3390/chemosensors12040056

Braitbart, O., Sasson, R., Weinreb, A. (1988) Mol. Cryst. Liq. Cryst., 159, 233-242.

Caplins, B.W., Mullenbach, T.K., Holmes, R.J., Blank, D.A. (2016) Femtosecond to nanosecond excited state dynamics of vapor deposited copper phthalocyanine thin films, Phys. Chem. Chem. Phys. 18 11454–11459.

Christie, R., & Abel, A. (2021). Phthalocyanine green pigments. 6(11), 665–669. https://doi.org/doi:10.1515/psr-2020-0193.

Claessens, C. G., González-Rodríguez, D., & Torres, T. (2002). Subphthalocyanines: Singular Nonplanar Aromatic CompoundsSynthesis, Reactivity, and Physical Properties. Chemical Reviews, 102(3), 835-854. https://doi.org/10.1021/cr0101454

Demir, S., Akbay, S., Canımkurbey, B., & Yuksel, F. (2024). Novel copper (II) phthalocyanines as semiconductor layer in organic field effect transistors: Synthesis and investigation of electrical properties. Journal Of Molecular Structure, 1308, 137981. https://doi.org/10.1016/j.molstruc.2024.137981

El-Saady, A. A., Roushdy, N., Farag, A. A. M., El-Nahass, M. M., & Basset, D. M. A. (2023). Exploring the molecular spectroscopic and electronic characterization of nanocrystalline Metal-free phthalocyanine: a DFT investigation. Optical And Quantum Electronics, 55(7). https://doi.org/10.1007/s11082-023-04877-8

Ezugwu, C. I., Kabir, N. A., Yusubov, M., & Verpoort, F. (2015). Metal–organic frameworks containing N-heterocyclic carbenes and their precursors. Coordination Chemistry Reviews, 307, 188-210. https://doi.org/10.1016/j.ccr.2015.06.012

Gounden, D., Nombona, N., & Van Zyl, W. E. (2020). Recent advances in phthalocyanines for chemical sensor, non-linear optics (NLO) and energy storage applications. Coordination Chemistry Reviews, 420, 213359. https://doi.org/10.1016/j.ccr.2020.213359

Gravano, S., Hassan, A. K., & Gould, R. D. (1991). Effects of annealing on the trap distribution of cobalt phthalocyanine thin films. International Journal of Electronics, 70(3), 477-484. https://doi.org/10.1080/00207219108921297

Hains, A. W., Liang, Z., Woodhouse, M. A., & Gregg, B. A. (2010). Molecular Semiconductors in Organic Photovoltaic Cells. Chemical Reviews, 110(11), 6689–6735. https://doi.org/10.1021/cr9002984

Kao, P., Chu, S., You, Z., Liou, S., & Chuang, C. (2005). Improved efficiency of organic light-emitting diodes using CoPc buffer layer. Thin Solid Films, 498(1-2), 249-253. https://doi.org/10.1016/j.tsf.2005.07.120Landi, S.,

Kobayashi, N. (2002). Design, Synthesis, Structure, and Spectroscopic and Electrochemical Properties of Phthalocyanines. Bulletin of the Chemical Society of Japan, 75(1), 1-19. https://doi.org/10.1246/bcsj.75.1

Kudrevich, S. V., & Van Lier, J. E. (1996). Azaanalogs of phthalocyanine: syntheses and properties. Coordination Chemistry Reviews, 156, 163-182. https://doi.org/10.1016/s0010-8545(96)01251-9

Kumar, A., Meunier-Prest, R., & Bouvet, M. (2020). Organic Heterojunction Devices Based on Phthalocyanines: A New Approach to Gas Chemosensing. Sensors, 20(17), 4700. https://doi.org/10.3390/s20174700

Landi, S., Segundo, I. R., Freitas, E., Vasilevskiy, M., Carneiro, J., & Tavares, C. J. (2021). Use and misuse of the Kubelka-Munk function to obtain the band gap energy from diffuse reflectance measurements. Solid State Communications, 341, 114573. https://doi.org/10.1016/j.ssc.2021.114573

Lee, H., Lee, J., Jeong, K., Yi, Y., Lee, J. H., Kim, J. W., & Cho, S. W. (2012). Hole Injection Enhancements of a CoPc and CoPc:NPB Mixed Layer in Organic Light-Emitting Devices. The Journal of Physical Chemistry C, 116, 13210-13216. https://doi.org/10.1021/jp3029598

Liu, L., Zhang, X. (2022) The excited state behavior of Group IA alkaline-metal phthalocyanines revealed by photoluminescence and singlet oxygen formation. Spectrochimica Acta Part A: Molecular and Biomolecular Spectroscopy 264 120297

Ma, Z., Zhao, J., Wang, X., & Yu, J. (2015). Effect of bulk and planar heterojunctions-based charge generation layers on the performance of tandem organic light-emitting diodes. Organic Electronics, 30, 136-142. https://doi.org/10.1016/j.orgel.2015.12.020

Miao, Q., Chi, X., Xiao, S., Zeis, R., Lefenfeld, M., Siegrist, T., Steigerwald, M. L., Nuckolls, C., Am. J., (2006). Chem. Soc., 128, 1340-1345

Muranaka, A., & Uchiyama, M. (2020). Development of Phthalocyanine-Based Functional Molecules with Tunable Optical and Chiroptical Properties. Bulletin of the Chemical Society of Japan, 94(3), 872-878. https://doi.org/10.1246/bcsj.20200336

Özdemir, M., Altinisik, S., Köksoy, B., Canımkurbey, B., Koyuncu, S., Durmuş, M., Bulut, M., & Yalçın, B. (2022). New metallophthalocyanines

including benzylphenoxy groups and investigation of their organic-field effect transistor (OFET) features. Dyes And Pigments, 200, 110125. https://doi.org/10.1016/j.dyepig.2022.110125

Cranston, R.R., Lessard, B.H. (2021) Metal phthalocyanines: thin-film formation, microstructure, and physical properties. RSC adv., 11, 21716-21737.

Stübinger, T., Brütting, W., (2001) Exciton diffusion and optical interference in organic donor–acceptor photovoltaic cells, J. Appl. Phys. 90, 3632–3641.

Tauc, J. (1968). Optical properties and electronic structure of amorphous Ge and Si. Materials Research Bulletin, 3(1), 37-46. https://doi.org/10.1016/0025-5408(68)90023-8

Tauc, J., & Menth, A. (1972). States in the gap. Journal Of Non-Crystalline Solids, 8-10, 569-585. https://doi.org/10.1016/0022-3093(72)90194-9

Thomas, G. (1997). Invisible circuits. *Nature*, *389*(6654), 907-908. https://doi.org/10.1038/39999

Wager, J. F. (2017). Real- and reciprocal-space attributes of band tail states. AIP Advances, 7(12). https://doi.org/10.1063/1.5008521

Yabaş, E., Biçer, E., & Katırcı, R. (2021). Experimental and In Silico studies on optical properties of new thiadiazole tetrasubstituted metal-free and zinc phthalocyanine compounds. Optical Materials, 122, 111808. https://doi.org/10.1016/j.optmat.2021.111808

Yu, T., Liu, L., Xie, Z., Ma, Y., (2015) Progress in small-molecule luminescent materials for organic light-emitting diodes, Sci. China: Chem. 58, 907–915.

Zhang X. et al. (2020) Molecular engineering of dispersed nickel phthalocyanines on carbon nanotubes for selective CO 2 reduction. Nat Energy

Zhu, L., Tang, H., Harima, Y., Kunugi, Y., Yamashita, K., Ohshita, J., & Kunai, A. (2001). A relationship between driving voltage and the highest occupied molecular orbital level of hole-transporting metallophthalocyanine layer for organic electroluminescence devices. Thin Solid Films, 396(1-2), 214-219. https://doi.org/10.1016/s0040-6090(01)01232-9